IEEE Open Journal of
Power Electronics

Received 13 June 2022; revised 28 July 2022; accepted 1 August 2022. Date of publication 9 August 2022; date of current version 16 August 2022. The review of this article was arranged by Associate Editor Lijun Hang.

Digital Object Identifier 10.1109/OJPEL.2022.3197545

A Ćuk-Based Modular DC–DC Converter For Medium Voltage Direct Current (MVDC) Applications

ABDULGAFOR ALFARES [1,2] (Member, IEEE), BRAD LEHMAN [1] (Senior Member, IEEE), AND MAHSHID AMIRABADI [1] (Senior Member, IEEE)

[1]Department of Electrical and Computer Engineering, Northeastern University, Boston, MA 02115 USA
[2]Department of Electrical Engineering, University of Hafr Albatin, Hafr Albatin 39524, Saudi Arabia

CORRESPONDING AUTHOR: ABDULGAFOR ALFARES (e-mail: abdulgafor.alfares@gmail.com)

An earlier version of this paper was presented in part at the "A modular SCR-based DC-DC converter for medium-voltage direct-current (MVDC) grid applications," presented at the IEEE Energy Conversion Congress and Exposition (ECCE) in 2017. [DOI: 10.1109/ECCE.2017.8096870].

ABSTRACT A highly reliable modular DC-DC converter that is well-suited to the medium -voltage direct-current (MVDC) grid applications is presented in this paper. Each power module in the proposed converter is designed and controlled such that it employs two small film capacitors for transferring the power from the source to the load. This feature eliminates the need for large electrolytic capacitors that are sensitive to high temperatures and have high failure rates. Furthermore, each power module is configured as an isolated converter, using an integrated high frequency transformer. Taking advantage of the leakage inductance of the transformer, the switches benefit from zero current turn-off and soft turn-on. Each power module sees only one switch or diode on the conduction path when transfering energy from the input to the link capacitors or from the link capacitors to the output, which results in relatively low conduction losses. Another advantage of the proposed converter is the possibility of having bidirectional flow of power. To form modular converters that facilitate sharing voltage or current in high power applications, the input terminals and output terminals of the power modules can be connected in series or in parallel. In this paper, an input-parallel output-series (IPOS) modular configuration is considered to increase the voltage blocking capability at the output and handle high currents at the input of the converter. In this paper, principles of the operation, design, and analysis of the proposed modular converter are discussed in detail, and performance of the modular converter is evaluated through simulations and experiments.

INDEX TERMS DC-DC converter, zero current switching (ZCS), medium -voltage direct-current (MVDC), modular converter.

I. INTRODUCTION

MEDIUM-Voltage (MV) grid is typically used as an interface between various renewable energy sources and different loads. MV grids, as depicted in Fig. 1, may also be used as a link between renewable energy sources and high-voltage direct-current (HVDC) transmission system [1]. There are two main approaches for stepping up the low input voltages to medium voltages in MV grid: The first approach establishes Medium Voltage AC (MVAC) grids by using low frequency transformers with large turn-ratios, as shown in Fig. 1(a) [2], [3], [4], [5]. However, high-voltage transformers that have large turn ratios are costly and have low power density. The second approach forms a Medium Voltage DC (MVDC) grid by employing DC-DC converters with high voltage gains, as represented in Fig. 1(b). This approach eliminates the need for large low frequency transformers. High-power efficient DC–DC converters that can offer large voltage gains are one of the key components of the MVDC grid [6], [7]. Different types of DC-DC converters have been proposed and studied for MVDC application. Some of these converters are single

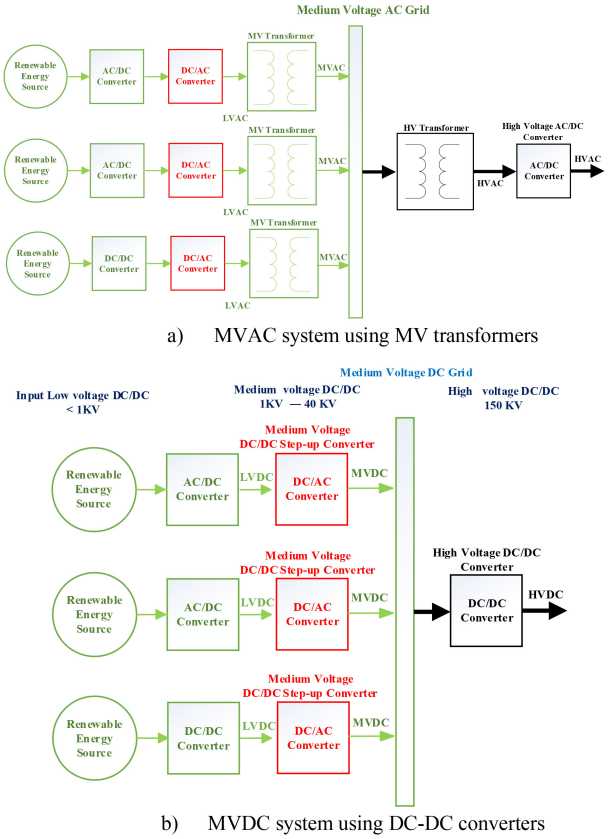

FIGURE 1. An example of MV grid used as a link between renewable energy sources/energy storage and an HVDC transmission system. a) MVAC system using MV transformers. b) MVDC system using DC-DC converters.

module configurations [4], [7], [8], [9], [10], [11], [12], [13], [14]. Soft-switching techniques are typically used in these converters to minimize the switching losses. However, in these converters power switches typically suffer from extremely high voltage stress. Considering the limitations of commercially available semiconductor devices, series connection of switches seems inevitable in most of these topologies. However, the voltage balancing across series switches is challenging. Additionally, the series connection of the switches can lead to more complex gate driver design [15].

Another category of DC-DC converters used in MVDC grid are modular converters, which are formed by several low power converters with series or parallel input/output terminals [16]. Modular converters are excellent candidates for MVDC grid application. Modular DC-DC converters allow the development of high-power rating converters using commercially available switches that have lower voltage/current ratings than input or output voltages/currents. These converters decrease the voltage stress (dv/dt) and problems associated with the electromagnetic interference (EMI). They also reduce the total harmonic distortion [17], [18], [19], [20], [21], [22], [23], [24]. Another major merit of modular DC-DC converters is the redundancy feature that allows them to operate under fault conditions, as each power module or power cell can work independently [25]. Additionally, maintenance of modular converters is expected to be easier [15]. Different modular DC-DC converter topologies are proposed in literature for MVDC applications. The most common topology used for developing modular DC-DC converters is Dual Active Bridge (DAB) converter [26]. A DAB converter is formed by an inductor, a medium frequency transformer, and two full bridges. DAB-based modular DC-DC converters offer numerous advantages such as soft switching capability and possibility of having bidirectional power flow. However, designing a high-power medium frequency transformer with large turns ratio and realizing soft-switching at all operating points can be challenging [26], [27], [28], [29]. Each power module in a DAB-based modular converter requires 8 switches, which increases total cost and make the control more complex. In modular DC-DC converters, depending on the input and output connections of modules, four basic configurations can be defined: input-parallel–output-series (IPOS), input- series – output-parallel (ISOP), input-series–output-series (ISOS), and input-parallel –output-parallel (IPOP). Among these combinations, the input-parallel – output-series (IPOS) configuration is more suitable for applications that require high output voltages, including MVDC grid [30].

Another type of modular DC-DC converter topology proposed for MVDC grid is based on Modular Multilevel Converters (MMCs) [15] and [31]. MMCs were introduced in 2002 as a very promising inverter topology for high-voltage applications. Several DC-DC converters based on MMCs have been proposed in literature [32], [33], [34], [35], [36], [37], [38], [39]. A modular multilevel DC converter (M2DC) is among these converters [15] and [39]. This topology is more complex compared to DAB-based modular converters and requires more switches [15]. Additionally, the circulating current of M2DC can be high if it is designed for a high voltage gain, and this may lower the efficiency of the converter [15]. In [40], a soft-switching MMC-based modular DC-DC converter is proposed. The soft-switching scheme of this converter employs a quasi-square wave modulation, leading higher efficiency due to the soft switching. However, it has difficulties with dynamic performance, and with complexity of design and control.

Several resonant modular DC-DC converters have been proposed, too. In [41], a modular DC–DC converter topology using resonant cells is proposed. This converter benefits from a multistring arrangement of switches that lowers the voltage stress across the switches. The power cells are each an isolated step-up resonant configuration connected in series at the output, which leads to a high voltage gain. In [13] , each power cell is formed by combining a boost converter and a series-parallel resonant converter to allow the switches and diodes benefit from soft-switching. This topology does not require a transformer; thus, the cost and weight are expected to be lower. Despite offering high efficiency, resonance in power cells of [41] and [13] , also, results in complexity of control and higher values of switch peak current.

Considering the importance of modular DC-DC converters in Medium Voltage DC (MVDC) and the problems associated

with the existing approaches, there is a motivation to develop new modular DC-DC converter topologies with improved attributes. This paper proposes a new family of modular DC–DC converter topologies based on a soft-switching Ćuk-based converter. In the proposed modular converter, each power module is an isolated soft-switching bidirectional Ćuk converter that benefits from zero current switching (ZCS) at any operating point. Compared to a DAB converter, this converter requires a smaller number of switches. The zero-current turn-off of the switches in the proposed converter allows using any type of active switches, even Silicon Controlled Rectifiers (SCRs) that are naturally commuted switches. SCRs have numerous advantages over the other switches, including lower conduction losses, higher voltage and current ratings, lower cost, and higher reliability, which are all of particular importance in the MVDC grid applications. However, use of SCRs limits the switching frequency; thus, they are mostly appealing to high power systems. The main limitation of SCRs is that they cannot be turned off with gate signals and they have natural commutation. Adding zero current turn-off feature to a DC-DC Ćuk converter, enables the proposed modular DC-DC converters to use SCRs. The soft switching converter used as a power module in the proposed modular converter can be categorized as a Quasi-Square Wave Converter (QSWC) [42]. Unlike resonant converters, in which the link components resonate continuously, in quasi-square wave converters resonance occurs during only short switching intervals to facilitate soft-switching, and during the rest of the cycle their operation is similar to that of PWM converter. This results in lower current/voltage stress of the switches compared to resonant converters. Moreover, the Quasi-Square Wave Ćuk Converter is designed such that the link capacitance is very small, even for high power systems. If the resonating modes are neglected, the link capacitor voltage seems to operate in critical conduction mode. Another advantage of the QSW converters, is that only one auxiliary passive component is added to facilitate soft switching. In general, the advantages of QSW converters include zero voltage or zero current switching, high efficiency, small link energy storage element, and single-stage power conversion feature. In the proposed modular converter, the input terminals of the quasi-square wave Ćuk converters are connected in parallel while their output terminals are connected in series, forming an IPOS modular configuration for MVDC grid application. Depending on the specifications of the system and application, the input terminals of the power modules can be connected in series or parallel and the output terminals can be connected in series or parallel.

The main contributions of this paper are as follows:

1) For the first time modular DC-DC converters based on quasi-square wave Ćuk converters are proposed, studied, and evaluated;
2) The proposed converter is less complex than DAB-based, MMC-based, and resonant-based modular converters;
3) The switches of the proposed converter have lower current rating than resonant-based modular converters;
4) The proposed converter is capable of using any type of controllable semiconductor switches, including IGBTs, MOSFETs, and SCRs; employing SCRs leads to higher efficiency and lower cost in high power applications;
5) The soft-switching feature of the proposed converter improves the efficiency and minimizes problems associated with EMI;
6) The proposed converter can transfer power in both directions;
7) The proposed converter uses very small film capacitors for each module; this eliminates the need for electrolytic capacitors that have shorter lifetime than film capacitors;

The authors studied the principles of the operation of this converter in preliminary conference paper [43] and evaluated the performance of one power module, i.e., a DC-DC quasi-square wave Ćuk converter, through experiment. In this paper the performance of the converter is studied in more details. Additionally, alternative topologies for reducing the number of switches and passive components will be introduced in this paper. Moreover, the performance of the proposed modular converter with three power modules is evaluated through experiments for the first time in this paper. Section II of this paper, will study the principles of the operation of each power module and the modular configuration. Design and analysis will be discussed in Section III. Simulations and experimental results will be presented in Section IV. Efficiency analysis is discussed in Section V, and the proposed modular converter will be compared with a DAB-based modular converter in Section VI. The paper will be concluded in Section VII.

II. PRINCIPLES OF THE OPERATION

Fig. 2 illustrates the schematic of the proposed modular converter, formed by several power modules. Each power module forming this modular converter is an isolated soft-switching DC-DC Ćuk converter that can step up or step down the voltage.The behavior of all power modules of the proposed modular converter is identical in each mode of operation. As mentioned earlier, the proposed modular converter can employ controllable switches, including controllable switches such as IGBTs and MOSFETs, as well as SCRs, which are semi-controllable switches. Fig. 2(a) shows the modular converter with SCRs and Fig. 2(b) shows the converter with IGBTs. The output voltage of a classic non-isolated Ćuk converter is negative. In Fig. 2(a) the transformer windings are adjusted such that the output of each power module is positive. Clearly, the positive output voltage can be realized regardless of the type of switches that are employed. In Fig. 2(b) the output of each power module is negative. The link capacitors in each power module, C_1 and C_2 in Fig. 2(a) and (b), transfer the power from the input towards the output, and the link inductors, L_{r1} and L_{r2} in Fig. 2(a) and (b), facilitate zero current turn-off and soft turn-on. L_{r1} and L_{r2} are very small, and the leakage inductance of the transformer can play the role of these inductors. This implies that the soft switching can be provided at almost no cost.

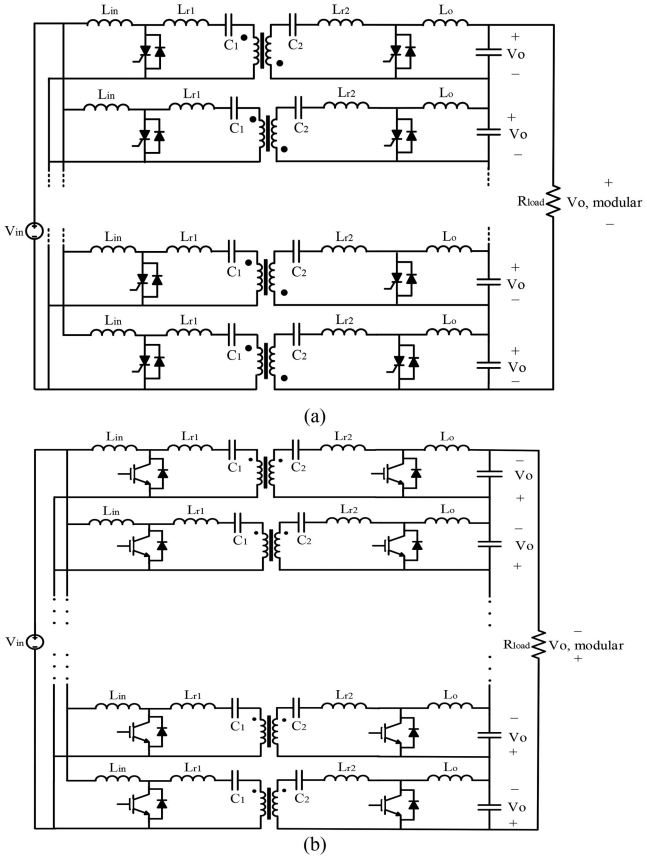

FIGURE 2. The proposed modular dc-dc converter that can use any time of switch (SCRs, MOSFETs, IGBTs): (a) with positive output voltage, (b) with negative output voltage.

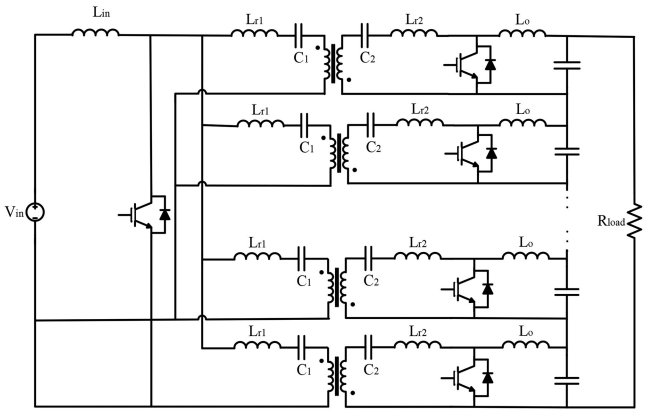

FIGURE 3. The proposed modular converter with reduced number of components.

Fig. 2 depicts IPOS modular configuration for handling a high input current and a high output voltage. If switches with high current rating to handle the input current are available, the modular configuration can be modified to reduce the number of components as depicted in Fig. 3.

The proposed modular converter also has the capability of interfacing several DC sources. The configuration shown in Fig. 4 is a multi-input modular converter that interfaces PV modules, batteries, and the MVDC line. The multi-input configuration can be realized by either the multi-input-switch configuration (Fig. 2) or the single-input-switch configuration (Fig. 3). The concept of MVDC is mainly used to collect the energy from different renewable sources and deliver it to the grid. Thus, the proposed multi-input configuration is an excellent candidate for this application.

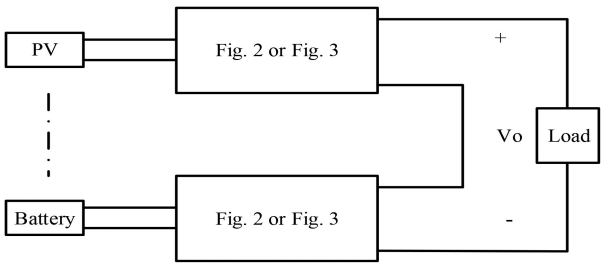

FIGURE 4. The proposed multi-input modular configuration.

As mentioned earlier each power module is, in essence, a quasi-square wave Ćuk converter. The main energy transfer elements are the link capacitors, and the inductors only create short resonating modes between charging and discharging of the link capacitors. If the resonating modes are neglected, the converter operates in Discontinuous Conduction Mode (DCM) or Critical Conduction Mode (CRM).

Operating the converter in CRM or DCM for the voltage or current of the main energy storage element also helps to achieve fast transient response and high power density and [44], [45], [46], [47], since smaller energy storage elements are required. Additionally, depending on the topology, the voltage or current of the main energy storage element reaches zero in CRM and DCM; therefore, a natural zero voltage/current switching can be realized [44], [45], [46], [47]. In QSW converters, an auxiliary passive component needs to be added to form partial resonant transients between the regular power transferring states of DC–DC PWM converters operating in CRM or DCM to improve the efficiency.

As depicted in Figs. 5 and 6, there are 4 modes in a switching cycle. The behavior of the converter during each modes is explained here:

- *Mode 1:* During Mode 1 (charging mode), switches S1 and S2 are off, and only diode D2 conducts. The link current (I_{Link}) is positive (from left to right) and is equal to the input current (I_{in} in Fig. 6). The positive link current charges the link capacitors during this mode, and the link voltage (V_{Link}) increases linearly. To end this mode, the input side switch (Switch S1) is turned on.
- *Mode 2:* This mode is a partial resonant mode during which both the output diode, D2, and the input switch, S, conduct, and the link elements (L_{r1}, L_{r2}, C_1, C_2) are shorted and resonate. During mode 2, the input switch current gradually increases from zero (zero current turn-on) while the output diode current, which is equal to the

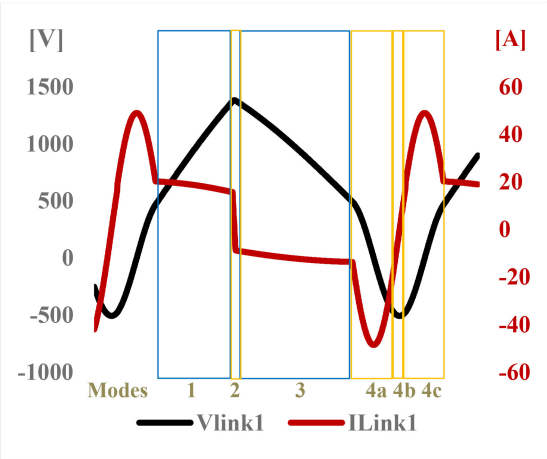

FIGURE 5. **Link current and voltage across C_1 of a power module in the proposed modular converter.**

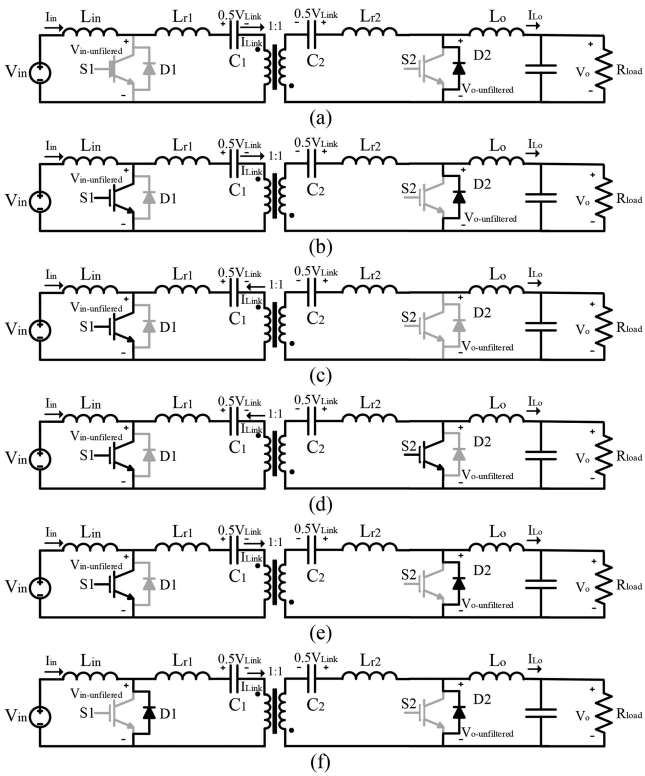

FIGURE 6. **The behavior of the proposed power module during different modes of operation, (a) mode 1, (b) mode 2, (c) mode 3, (d) mode 4a, (e) mode 4b, (f) mode 4c.**

sum of input and output currents, $I_{In}+I_{Lo}$, at the beginning of this mode, decreases. The link current, which is equal to the input current at the beginning of mode 2, also decreases during this mode, and its polarity changes. The slope of current increase/decrease and duration of mode 2 depend on the link inductance, i.e., $L_{r1}+L_{r2}$. When the current of diode D2 becomes zero, Mode 3, which is the discharging mode, starts. At the end of mode 2 the link current is equal to - I_{Lo}.

- *Mode 3:* During mode 3 (discharging mode), the link current is negative (from right to left), and its absolute value is equal to the output current, I_{Lo}. Due to the negative polarity of link current the link capacitors are discharged and the link voltage decreases. The link voltage decreases until it is close to zero. Mode 3 is ended before the link capacitors are fully discharged, since the link capacitors must have sufficient energy to allow the link current to swing to the input current. To end this mode, the output switch, S2, is turned on, and this initiates the second resonating mode, Mode 4.
- *Mode 4:* Mode 4 can be divided into three stages. During the first stage of this mode (Mode 4a), both the input switch and output switch conduct, the link elements are shorted, and the absolute value of the link current, which is negative, increases until it reaches its peak value, and then it decreases. When the absolute value of the link current becomes equal to the output current again ($I_{Link}=-|I_{Lo}|$), the current of switch S2 becomes zero and this switch is turned off. This initiates the second stage of mode 4 (Mode 4b) during which switch S1 and diode D2 conduct. In case MOSFETs or IGBTs are used, switch S2 can be turned off after Mode 4b starts. Clearly, if SCRs are used, the switch will automatically turn off when its current becomes zero. The link current increases during Mode 4b and becomes positive. Once it becomes equal to the input current ($I_{Link}=|I_{In}|$), switch S1 stops conducting, and diode D1 starts to conduct. At this point Mode 4c starts during which only diodes D1 and D2 conduct. Link current continues to increase during Mode 4c until it reaches a peak value, and after that it decreases. Mode 4c ends when the link current, which is higher than the input current during this mode, becomes equal to the input current. At this moment, diode D1 stops conducting, and mode 1 of the following cycle starts. If MOSFETs or IGBTs are used instead of SCRs, switch S1 must be turned off during Mode 4c; otherwise, the link inductors and capacitors will continue resonating after Mode 4c.

Fig. 7 depicts the equivalent circuit of the proposed power module during each mode of operation.

The input-side diode (D1) can be removed. In this case, Mode 4c will be eliminated and Mode 4 will be shorter, which is desirable; however, for applications that require bidirectional flow of power, both switches and both diodes are needed.

In the proposed modular configuration, all power modules are controlled such that they all have the same operation.

III. DESIGN AND ANALYSIS

To design and analyze the proposed modular converter, initially a single power module will be analyzed.

A. POWER MODULE ANALYSIS

As mentioned earlier each power module in the proposed modular converter is in essence a quasi-square wave Ćuk

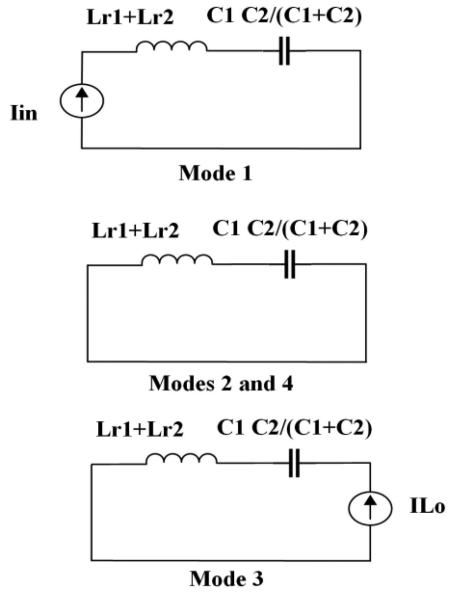

FIGURE 7. The equivalent circuit of each power module during modes 1 to 4.

converter. In this converter, the resonant modes (Modes 2 and 4) are typically much shorter than charging and discharging modes (Modes 1 and 3); therefore, they can be ignored when designing the converter. The link capacitance is determined such that the link capacitor voltage of the hard-switching converter is in CRM. This increases the link capacitors peak voltage; however, it allows using very small link capacitors. Due to this this feature film capacitors, which have longer lifetime compared to electrolytic capacitors, can be used in this converter. It can be shown that the link capacitance in each isolated power module (C_1=C_2) has the following relationship with the switching frequency (f), rated power of each power module (P), input voltage of each power module (V_{in}), and the output voltage of each power module (V_{o}):

$$\text{C}_1 = \text{C}_2 = 2\text{C}_{\text{link}} = \frac{\text{P}}{\text{f}(\text{V}_{\text{in}} + \text{V}_{\text{o}})^2} \tag{1}$$

In (1), C_{link} is the equivalent link capacitance in each power module. To make sure resonant modes are much shorter than the power transfer modes, the equivalent link inductance of an isolated power module, $L_{r,eq}$, where $L_{r,eq} = 2L_{r1} = 2L_{r2}$, can be determined by (2):

$$\frac{1}{2\pi\sqrt{C_{link}L_{r,eq}}} \gg f \tag{2}$$

If the resonant modes are neglected, the peak value of the link voltage, which is the sum of voltages across C_1 and C_2, can be calculated based on the input voltage and output voltage of each power module, as follows:

$$V_{link,\ p} = 2\,(\,V_{in} + \ V_o) \tag{3}$$

To determine the voltage gain ratio in a power module, resonating modes can be neglected. The unfiltered input voltage is equal to the link voltage during mode 1, and it is zero in other modes. Similarly, the unfiltered output voltage is equal to the link voltage in mode 3 and it is zero during other modes. The average of the unfiltered input voltage, which is equal to V_{in}, can be determined as:

$$V_{in} = \frac{1}{2T}\,(V_{link,\ p}\,t_{charging})f \tag{4}$$

The average of the unfiltered output voltage, which is equal to V_{o}, is determined as follows:

$$V_o = \frac{1}{2T}\,(V_{link,\ p}\,t_{discharging})f \tag{5}$$

The voltage gain can be determined as:

$$\frac{V_o}{V_{in}} = \frac{t_{charging}}{t_{discharging}} \tag{6}$$

It can be shown that the above relationship between input and output voltages is valid even when resonant modes are taken into consideration. Assuming D is the duty cycle of the input side switch, according to Section II:

$$D = \frac{t_{discharging}}{T} \tag{7}$$

$$1 - D = \frac{t_{charging}}{T} \tag{8}$$

From (6)–(8) the voltage gain can be calculated as when the resonant modes are neglected:

$$\frac{V_o}{V_{in}} = \frac{D}{1-D} \tag{9}$$

This was indeed expected since each submodule is in essence a Cuk-based converter.

To find the duration of conduction of each switch in the soft-switching converter, the LC resonant circuits during modes 2 and 4 can be solved.

B. ANALYSIS OF THE PROPOSED MODULAR CONVERTER

To determine the number of required power modules in a modular converter, the current and voltage stress of each switch in a power module need to be determined. Here it is assumed that the limiting factor is the low voltage rating of the switches rather than their low current rating. The peak voltage across the switches in a power module, $V_{S,peak}$, is equal to the link peak voltage $V_{link,\ p}$:

$$V_{S,peak} = V_{link,\ p} \tag{10}$$

The voltage rating of the selected switches, $V_{S,rated}$, needs to be higher than $V_{S,peak}$. Considering an IPOS modular converter formed by "N" power modules, the output voltage of the modular converter, $V_{O\_modular}$, is as follows:

$$V_{O\_modular} = N\ \times V_O \tag{11}$$

$$V_{O\_modular} = N\ \times \frac{D}{1-D} \times\ V_{in} \tag{12}$$

The input voltage of the IPOS modular converter is the same as the input voltage of each power module.

Using (3), (10) and (11), the number of required power modules, N, can be determined by (13):

$$\mathrm{N} \geq \frac{2 \times V_{O\_modular}}{V_{S,rated} - 2V_{in}} \tag{13}$$

According to (13) the number of required power modules depends on the input and output voltages of the modular converter and the voltage rating of the available switches ($V_{S,rated}$). If the voltage rating of the switches ($V_{S,rated}$) is lower than $2V_{in}$, the input terminals of the power modules cannot be connected in parallel, and an input-series output-series modular configuration is needed.

The equivalent link capacitance (C_{link}) in each power module can be determined by (14):

$$C_{link} = \frac{2P_{modular\_rated}}{N \times V_{S,peak}^2 f} \tag{14}$$

where $P_{modular\_rated}$ is the rated power of the modular configuration.

The proposed modular converter requires 2N switches and 2N capacitors. According to (14), the link capacitance is very small in this modular converter. For instance, in a system with $P_{modular\_rated}$ =1 MW, $\mathrm{V_{in}}$=1000 V, f=5 kHz, and $\mathrm{V_{S,rated}}$=5 kV, $V_{O\_modular}$ = 37.5 kV , the number of required capacitors and switches will be 50, and the capacitance of each capacitor will be 1.28 μF.

As mentioned earlier, when switches with high current ratings are available, the proposed converter can be modified as depicted in Fig. 3 to lower the number of switches to N+1 in this converter. The reduction of switch and passive components count improves power density of topology shown in Fig. 3 compared to the topology illustrated in Fig. 2. However, the reduced switch topology has higher conduction losses than the original converter.

C. CURRENT AND VOLTAGE STRESS OF THE SEMICONDUCTOR DEVICES

The current stress of the input and output switches in the original and reduced switch configurations are as follow:

$$I_{sw,in,\ original} = \frac{I_i}{N} + I_o \tag{15}$$

$$I_{diode,out,\ original} = \frac{I_i}{N} + I_o \tag{16}$$

$$I_{sw,in,reduced\ switch} = I_i + NI_o \tag{17}$$

$$I_{diode,out,reduced\ switch} = \frac{I_i}{N} + I_o \tag{18}$$

where $\mathrm{I_i}$ and $\mathrm{I_o}$ are the input and output currents of the modular configuration.

The input side diode and output side switch conduct only during the resonant modes and their current is small.

The peak voltage across the input and output switches in each power module, which determines the voltage stress of the switches, is as follow:

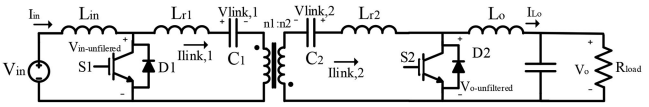

FIGURE 8. The schematic of the power module with unequal primary and secondary transformers turns.

$$V_{S,peak} = 2\,(V_{in} + V_o) = 2\left(V_{in} + \frac{V_{O\_modular}}{N}\right) \tag{19}$$

where V_{in} , V_o, $V_{O\_modular}$ are the input voltage of the modular converter, the output voltage of each module, and output of the modular configuration.

D. THE EFFECT OF TRANSFORMER TURN RATIO ON DESIGNING THE PROPOSED CONVERTER

It is possible to use transformers with unequal number of primary and secondary turns. The schematic of an isolated power cell with arbitrary primary and secondary transformer turns is shown in Fig. 8. As seen in this figure, turn ratio of the transformer, the voltage across primary capacitor, voltage across secondary capacitor, current of the primary capacitor, current of the secondary capacitor, capacitance of the primary capacitor, and capacitance of the secondary capacitor are denoted by $\frac{n_2}{n_1} = a$, Vlink,1, Vlink,2, Ilink,1, Ilink2, C1, and C2, respectively.

When the number of turns at the primary and secondary of the transformer are not equal, the link peak voltage of the primary and secondary capacitors will not necessarily be the same. During the charging mode the primary side and secondary side currents determine the peak voltage across the primary and secondary capacitors ($\mathrm{V_{link,P1}}$ and $\mathrm{V_{link,P2}}$):

$$I_{in} = \frac{\mathrm{C_1\ V_{link,P1}}}{\mathrm{t_{charging}}} \tag{20}$$

$$\frac{I_{in}}{a} = \frac{\mathrm{C_2\ V_{link,P2}}}{\mathrm{t_{charging}}} \tag{21}$$

During the discharging mode, the relationship between the primary and secondary currents and the peak voltages of the capacitors is as follows:

$$a\ I_{Lo} = \frac{\mathrm{C_1\ V_{link,P1}}}{\mathrm{t_{discharging}}} \tag{22}$$

$$I_{Lo} = \frac{\mathrm{C_2\ V_{link,P2}}}{\mathrm{t_{discharging}}} \tag{23}$$

From the above equations we can show

$$\mathrm{C_1\ V_{link,P1}} = a\mathrm{C_2\ V_{link,P2}} \tag{24}$$

If we select the following relationship between C1 and C2:

$$\mathrm{C_1} = a\mathrm{C_2} \tag{25}$$

Then

$$\mathrm{V_{link,P1}} = \mathrm{V_{link,P2}} \tag{26}$$

TABLE 1. Specifications of the Simulated System

Parameters	Values
Link capacitance in each power module ($C_1 = C_2$)	0.64 µF
Link inductor ($L_{r1} = L_{r2}$)	75 µH
Input Voltage (V_i)	500 V
Output voltage of each power module (V_o)	750 V
Total Power	100 kW
Switching frequency (f)	8 kHz
Number of power module	12

Vin and Vo are equal to the averages of the unfiltered input and output voltages and can be determined as follows:

$$V_{in} = \frac{1}{2T}\left(V_{link,\ p1}t_{charging} + \frac{V_{link,\ p2}t_{charging}}{a}\right) f = \frac{t_{charging}}{2T}\frac{a+1}{a}V_{link,\ p1} \quad (27)$$

$$V_o = \frac{1}{2T}\left(a\,V_{link,\ p1}t_{discharging} + V_{link,\ p2}t_{discharging}\right) f = \frac{t_{discharging}}{2T}\,(a+1)\,V_{link,\ p1} \quad (28)$$

Using the above equations, $V_{link,P1}$ can be determined based on the input and output voltages:

$$V_{link,\ p1} = V_{link,\ p2} = 2\left(\frac{a}{a+1}\ V_{in} + \frac{1}{a+1}\ V_o\right) \quad (29)$$

The peak voltage across the switches in primary and secondary side of the power module can be obtained as follows:

$$V_{S1} = \frac{a+1}{a}V_{link,\ p1} = 2\left(V_{in} + \frac{V_o}{a}\right) \quad (30)$$

$$V_{S2} = (a+1)\ V_{link,\ p1} = 2\,(aV_{in} + V_o) \quad (31)$$

The number of required power modules, N, can be determined by (16):

$$N = \frac{V_{O\_modular}}{\frac{V_{s\ ,\ rated}}{2} - aV_{in}} \quad (32)$$

By selecting a<1 the number of required power modules can be reduced.

IV. SIMULATION AND EXPERIMENTAL RESULTS

This section presents the simulation and experimental results corresponding to the proposed converter.

A. SIMULATION RESULTS

Both the original configuration (Fig. 2) and the reduced switch configuration (Fig. 3) have been simulated, and the results are presented in parts (A) and (B), respectively. In both cases IGBTs are used.

1) ORIGINAL TOPOLOGY

A 100-kW converter with specifications listed in Table 1 has been simulated in PSIM. Each power module handles about 8.3 kW and needs two small capacitors (C_1=C_2= 0.64 µF)

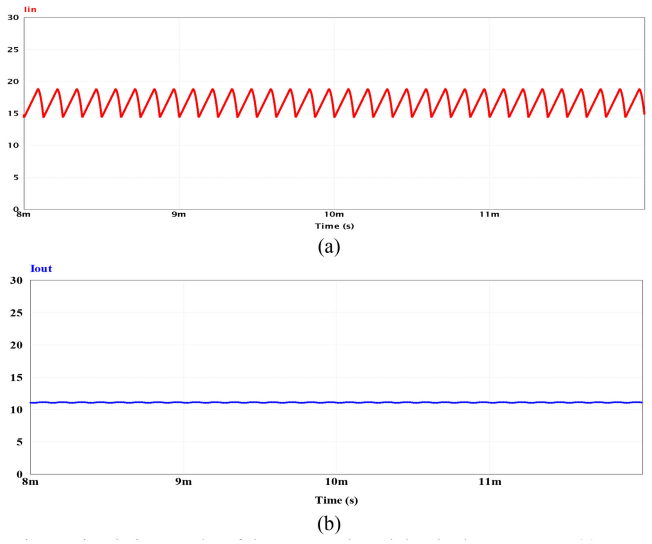

FIGURE 9. Simulation results of the proposed modular dc-dc converter: (a) Input current of a power module, (b) output current of a power modular.

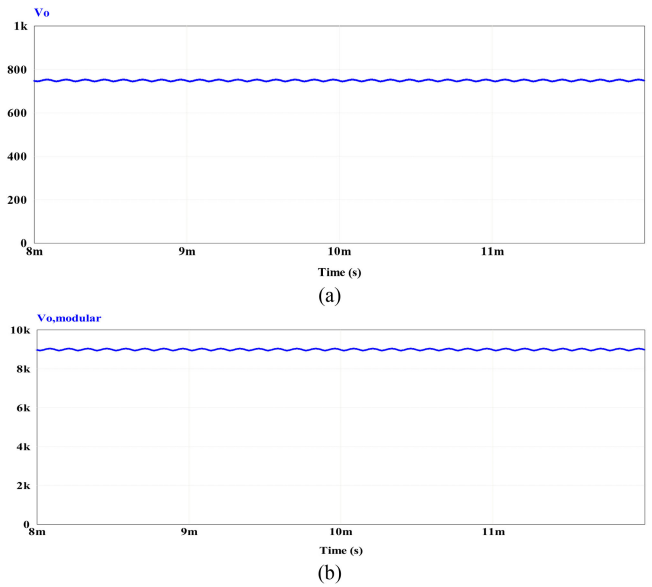

FIGURE 10. The output voltage of (a) each power module, (b) modular converter.

for transferring power from input to output. Figs. 9-11 represent the simulation results. The input and output currents of each power module are shown in Fig. 9. Since the input terminals of the power modules are connected in parallel, the input current of each module is equal to the input current of the modular converter divided by 12. The output current of each module is the same as the output current of the modular converter. Fig. 10 depicts the output voltge of each power cell as well as the output voltage of the modular converter, which is 9000 V. As expected, the output voltage of modular converter is 12 times the output voltage of each module, which 750 V. Fig. 11 shows the currents and voltages of the input

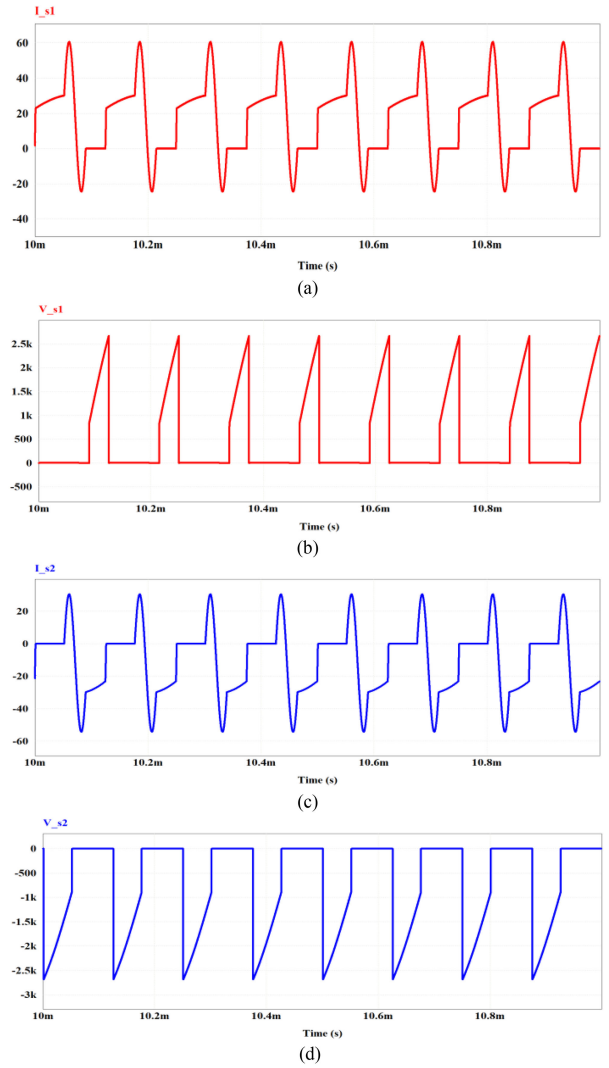

FIGURE 11. Simulation results of the proposed converter, (a) The current flowing through the input-side switch and diode, (b) The voltage across the input-side switch, (c) The current lowing through the output-side switch and diode, (d) The voltage across the output-side switch.

and output switches. Negative current of a switch implies that the anti-parallel diode is conducting. Zero current turn-off and soft turn-on of the switches is verified in Fig. 11.

2) REDUCED-SWITCH CONFIGURATION

The reduced switch configuration has also been simulated in PSIM. The specifications of the simulated converter are similar to those of the original configuration simulated in the previous part (parameters listed in Table 1). Fig. 12 displays the total output voltage of the modular converter, link current, and the voltage across the primary side capacitor. The output voltage is 9000 V and is identical to the output voltage of the original configuration. The peak voltage across the primary capacitor is half the link peak voltage . Fig. 13 depicts the current and voltage of the input switch. The input switch current is 12 times higher than that of the original configuration.

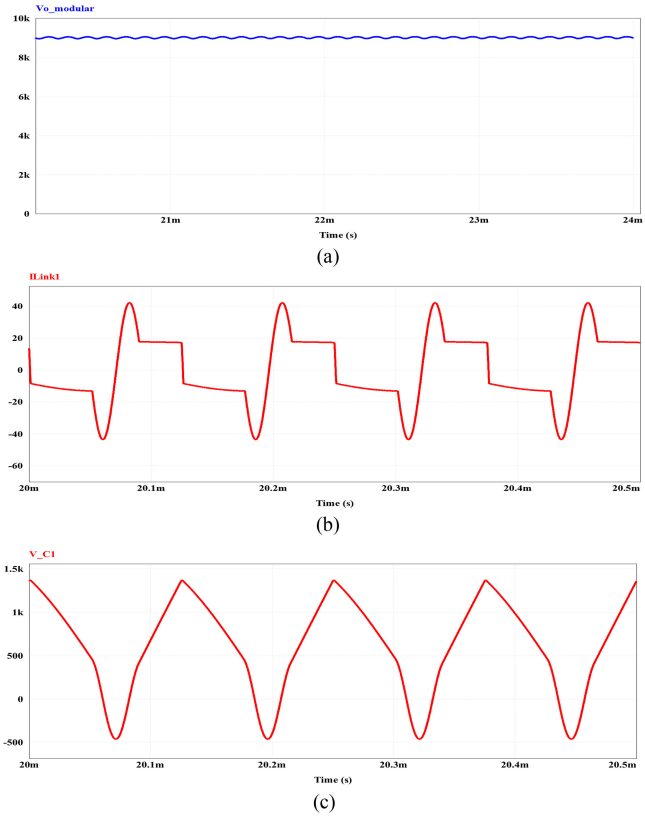

FIGURE 12. Simulation results of the proposed reduced switch converter: (a) Output voltage, (b) link current, and (c) voltage across C_1.

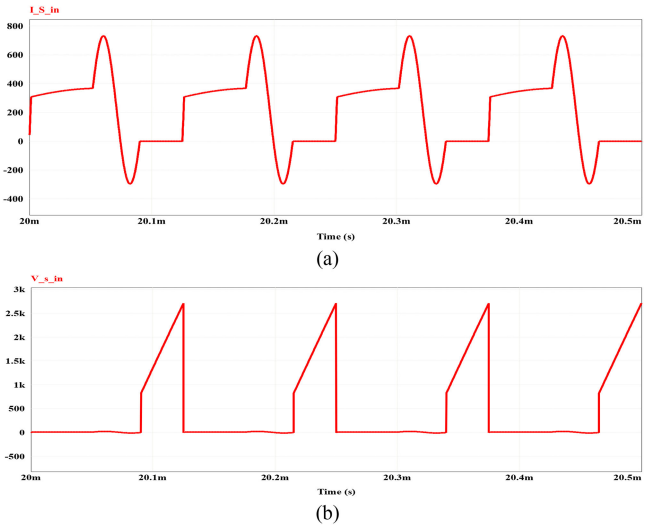

FIGURE 13. Simulation results of the proposed reduced switch converter: (a) Input current, (b) input switch current, and (c) input switch voltage.

B. EXPERIMENTAL RESULTS

In this section, two sets of experimental results are presented. In the first set of experiments the operation of a power module with SCRs is evaluated. In the second set of experiments the performance of the proposed modular converter with MOSFETs is evaluated.

TABLE 2. Specifications of the Hardware Setup for the 1st Experiment

Parameters	Values
Link Capacitance (C_{link})	5 µF
Link Inductor (L_r)	16 µH
Input Voltage (V_{in})	30 V
Power of the Power module (P)	108 W
Load Resistance	6.3 Ω
Switching Frequency (f)	3.3 kHz
SCR	TN4015H-6I

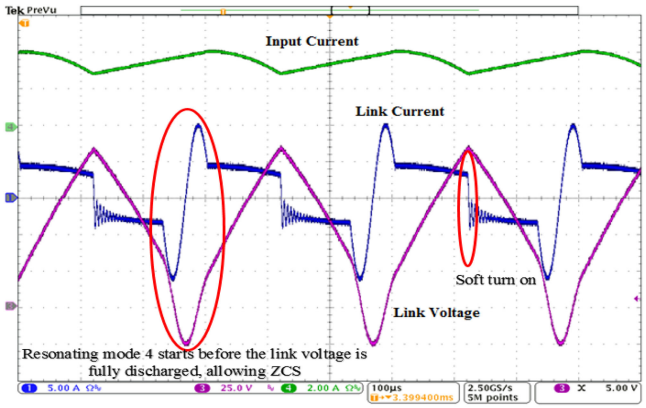

FIGURE 14. The experimental results corresponding to a single power module with SCRs: input current, voltage across the link capacitor, and link current.

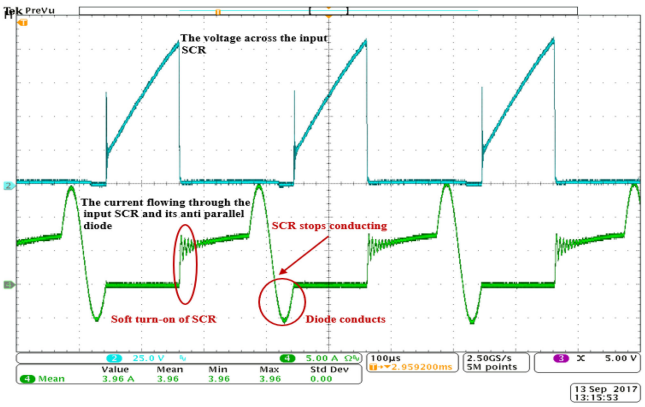

FIGURE 15. The experimental results corresponding to a single power module with SCRs: The voltage across the input-side switch, the current flowing through the input-side diode and SCR.

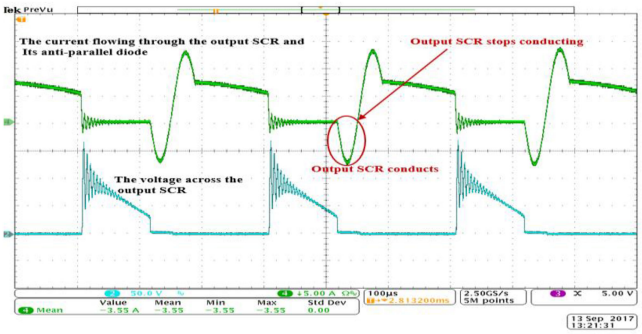

FIGURE 16. The experimental results corresponding to a single power module with SCRs: The voltage across the output-side switch, the current flowing through the output-side diode and the SCR.

1) SCR-BASED POWER MODULE

A low-power quasi-square-wave Ćuk converter with SCRs is implemented in hardware to validate the performance of the SCR-based power module in the proposed converter. A non-isolated configuration is tested in this part. The parameters of the converter are listed in Table 2.

Fig. 14 shows the input current, link voltage, and link current of the dc-dc converter. As seen in this figure, between each charging mode (Mode 1) and discharging mode (Mode 3) there is a resonant mode (Mode 2 or Mode 4), which realizes ZCS. As seen in Fig. 14, the peak value of the link capacitor voltage is 110 V. Fig. 15 depicts the voltage across the input-side SCR and the current flowing through the input-side SCR and its anti-parallel diode. This figure shows that during the first resonating mode (Mode 2) the SCR current starts increasing from zero, and it remains almost constant during the discharging mode (Mode 3). At the beginning of the second resonating mode (Mode 4), the current flowing through the SCR starts increasing, it reaches a maximum value, and then it decreases. Once the current becomes zero, the SCR stops conducting, and the input diode conducts after this point. Fig. 16 shows the voltage across the output-side SCR and the current flowing through the output-side SCR and its anti-parallel diode. A positive current in Fig. 16 implies the diode is conducting, and a negative current implies that the SCR conducts. As seen in Fig. 16, during Mode 1, the output diode current is almost constant, and during Mode 2, it decreases to zero. In Mode 4, initially the output-side SCR conducts for a short time, and then the output diode conducts. The voltage ringing seen in Fig. 16 occurs due to the resonance of link inductor and parasitic capacitors of the switches. A snubber can be used to eliminate this voltage ringing. The experiment further validated the description in Section II of the modes operation.

2) MOSFET-BASED MODULAR CONVERTER

A Modular converter formed by three power modules, as shown in Fig. 17, was designed and implemented in the hardware. Each power module is isolated and uses MOSFETs.

The parameters of the implemented system are listed in Table 3. Fig. 18 shows the total input current, input current of one power module, and output current of the modular converter. It can be observed from this figure that the total input current is 5.4 A, the input current of one of the power modules is 1.8 A, and the output current of the modular converter is 1.25 A.

Fig. 19 represents the voltage across the primary capacitor in each of the three power modules.

Fig. 20 illustrates the link current of the three power modules. It can be observed that the link currents of the power modules are identical, which is as expected.

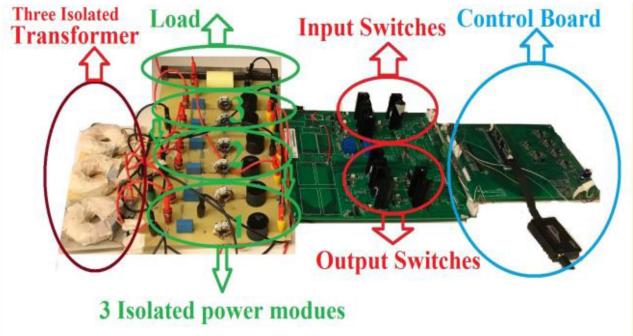

FIGURE 17. Hardware setup of the modular converter.

TABLE 3. Specifications of the Hardware Setup for the 2nd Experiment

Parameters	Values
Link Capacitance ($C_{1,2}$)	10 µF
Link Inductor ($L_{r1,2}$)	11 µH
Input Voltage (V_{in})	20 V
power of the Power Modular (P)	108 W
Output Voltage (V_{out})	75V
Switching Frequency (f)	5 kHz
MOSFET	SUP90330E-GE3
Efficiency	87 %

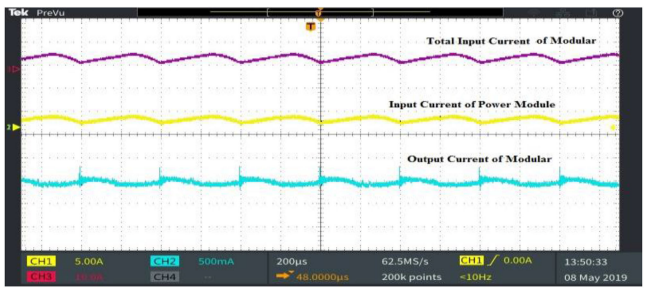

FIGURE 18. The experimental results corresponding to modular converter with three power modules: the total input current of Module, Input current of power module, and output current of Modular.

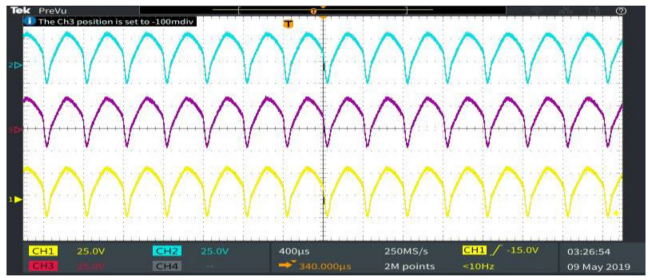

FIGURE 19. The experimental results corresponding to modular converter with three power modules: the three link voltages in each of the power module.

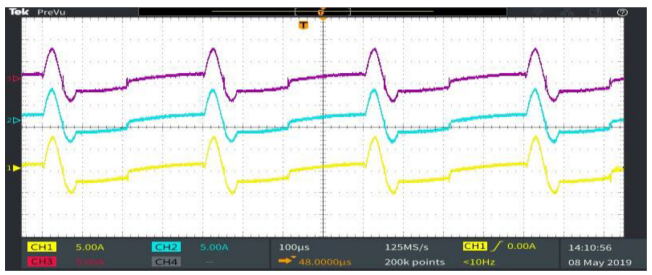

FIGURE 20. The experimental results corresponding to modular converter with three power modules: link currents in each of the power module.

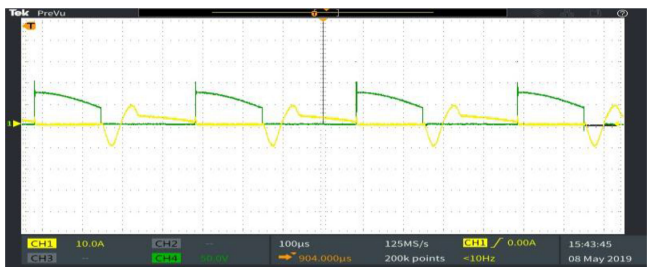

FIGURE 21. The experimental results corresponding to modular converter with three power modules: The voltage across the input-side switch, the current flowing through the input-side switch and its anti-parallel diode.

Fig. 21 depicts the voltage across the input-side switch and the current flowing through the input-side switch and its anti-parallel diode in one of the power modules. Fig. 22 depicts the voltage across the output -side switch and the current flowing through the output-side switch and its anti-parallel diode in one of the power modules. According to (3) and (10), the peak voltage of each switch is approximately twice the sum of input and output voltages of a power module. As seen in Figs. 21 and 22, the peak value of the voltages across these switches is around 80 V.

Fig. 23 represents the output voltage of the power modular, which is 75 V.

V. EFFICIENCY ANALYSIS

This section analyzes the efficiency of the proposed converter. In the proposed modular converter, the switching losses are negligible and conduction loss of the switches, transformer loss, and filter loss are major sources of power dissipation. The measured efficiency of the modular converter tested in part B2 of Section IV is 87%. To determine the power loss breakdown, accurate models of the components were used in PSIM and the modular converter was simulated. Fig. 24 depicts the power loss breakdown. The measured efficiency of the converter and the efficiency determined through accurate simulations are very close. To show that the efficiency of the proposed converter increases at higher power level, simulations with accurate component models were carried out for a number of operating points, and as seen in Fig. 25, the efficiency reaches 91.4% at 400 W.

VI. COMPARISON TO DAB-BASED MODULAR CONVERTER

As mentioned earlier, DAB-based modular converter is the most common modular DC-DC converter. In this section the proposed modular converter is compared with a DAB-based modular converter. Table 4 compares the number of passive

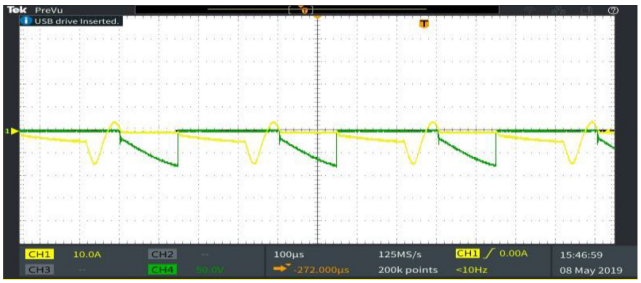

FIGURE 22. The experimental results corresponding to modular converter with three power modules: The voltage across the output-side switch, the current flowing through the output-side switch and its anti-parallel diode.

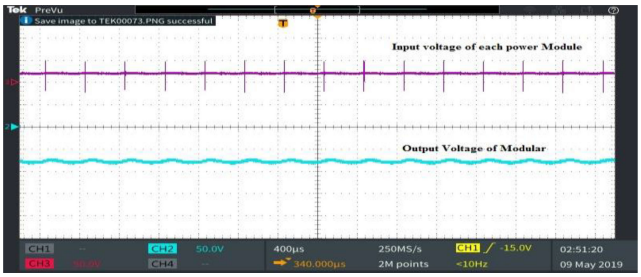

FIGURE 23. The experimental results corresponding to modular converter with three power modules: the output voltage of the modular converter, and input voltage of each power module.

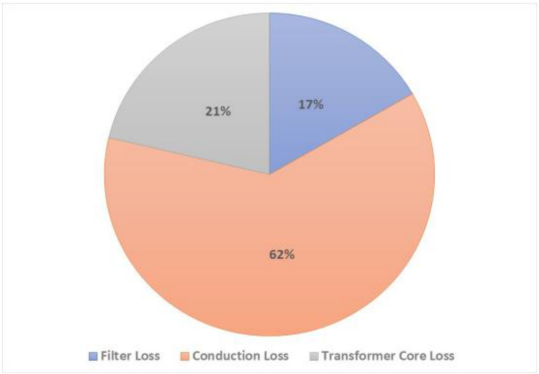

FIGURE 24. Power loss breakdown at 108 W.

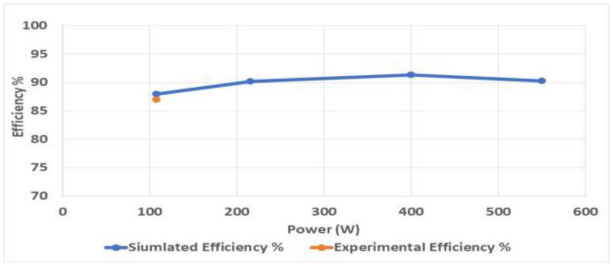

FIGURE 25. Efficiency curve.

TABLE 4. Comparison of the Modular Converters

Cell type	DAB-Based modular converter	Proposed modular converter
Topology	[26]	Proposed
Schematic	Fig. 2 of [26]	Fig. 2
Input voltage	500	500
Output voltage of each power module	2250	750
Number of passive elements to obtain soft switching	32	24
Number of power modules	4	12
Number of switches	32	24
Peak value of the voltage across switches	2250 V	2500 V
Number of switches on the conduction path	4	1
Power rating of each power module	25 kW per power module	8.33 kW per power module
Efficiency (simulated)	96.7 %	98.7%

elements, number of power modules, number of switches, voltage stress across the switches, number of switches on the conduction path, power rating of each power module, and the efficiency of the two converters. The converters are designed assuming the acceptable peak voltage across the switches is between 2000 V and 2500 V. To achieve output voltage of 9000 V, four power modules that have total of 32 switches are needed in a DAB-based modular converter while the proposed converter requires 24 switches.

Comparison of the two converters can be summarized as follows:

- The number of switches in DAB-based modular converter is more than the number of switches in the proposed converter.
- The total conduction losses of the switches in DAB-based converter is higher than that of the proposed topology.
- As mentioned before, DAB-based modular converter does not offer soft-switching for all operating points
- If a fault occurs in one of the power modules of the DAB-based modular converter, this fault may cause losing 25 kW of power while a fault in one of the modules of the proposed topology, will cause losing 8.33 kW of power.

As listed in in Table 4, the simulated efficiency of the proposed converter is 98.7% at 100 kW while the efficiency of DAB-based converter is 96.7%. The efficiency was calculated

by considering only the conduction losses. The conduction losses in DAB-based converter is obtain from [48].

VII. CONCLUSION

A Ćuk-Based Modular DC–DC converter is proposed in this paper for MVDC application. The unique features of this new modular DC-DC converter are as follows: First, each power module uses small film capacitors, which make this modular converter reliable. Second, each power module in the proposed modular converter is a soft-switching bidirectional Ćuk-based converter that promises zero current switching (ZCS) at any operating point, and this leads to an efficient modular converter. Third, SCRs can be used in this converter. The proposed modular converter can employ controllable switches, including IGBTs and MOSFETs, or SCRs, which are semi-controllable switches. SCRs are low-cost, reliable, and efficient, and are preferable for some high-power applications. Being modular, this converter has a large conversion ratio. This paper presents the principles of the operation of the proposed modular converter as well as the design procedure. Moreover, a reduced-switch configuration based on the proposed topology is introduced in this paper. Simulations and experimental results are presented to evaluate the performance of the proposed converter.

REFERENCES

[1] Y. Hu, R. Zeng, W. Cao, J. Zhang, and S. J. Finney, "Design of a modular, high step-up ratio DC–DC converter for HVDC applications integrating offshore wind power," *IEEE Trans. Ind. Electron.*, vol. 63, no. 4, pp. 2190–2202, Apr. 2016, doi: 10.1109/TIE.2015.2510975.

[2] M. T. Daniel, H. S. Krishnamoorthy, and P. N. Enjeti, "A new wind turbine interface to MVdc collection grid with high-frequency isolation and input current shaping," *IEEE J. Emerg. Sel. Top. Power Electron.*, vol. 3, no. 4, pp. 967–976, Dec. 2015, doi: 10.1109/JESTPE.2015.2443843.

[3] N. Denniston, A. M. Massoud, S. Ahmed, and P. N. Enjeti, "Multiple-Module high-gain high-voltage DC–DC transformers for offshore wind energy systems," *IEEE Trans. Ind. Electron.*, vol. 58, no. 5, pp. 1877–1886, May 2011, doi: 10.1109/TIE.2010.2053340.

[4] H. Athab, A. Yazdani, and B. Wu, "A transformerless DC–DC converter with large voltage ratio for MV DC grids," *IEEE Trans. Power Del.*, vol. 29, no. 4, pp. 1877–1885, Aug. 2014, doi: 10.1109/TPWRD.2013.2297431.

[5] J. Robinson, D. Jovcic, and G. Joós, "Analysis and design of an offshore wind farm using a MVDC grid," *IEEE Trans. Power Del.*, vol. 25, no. 4, pp. 2164–2173, Oct. 2010.

[6] S. Cui, N. Soltau, and R. W. De Doncker, "A high step-up ratio soft-switching DC–DC converter for interconnection of MVDC and HVDC grids," *IEEE Trans. Power Electron.*, vol. 33, no. 4, pp. 2986–3001, Apr. 2018, doi: 10.1109/TPEL.2017.2702207.

[7] W. Chen, A. Q. Huang, C. Li, G. Wang, and W. Gu, "Analysis and comparison of medium voltage high power DC/DC converters for offshore wind energy systems," *IEEE Trans. Power Electron.*, vol. 28, no. 4, pp. 2014–2023, Apr. 2013, doi: 10.1109/TPEL.2012.2215054.

[8] C. Meyer, M. Hoing, A. Peterson, and R. W. De Doncker, "Control and design of DC grids for offshore wind farms," *IEEE Trans. Ind. Appl.*, vol. 43, no. 6, pp. 1475–1482, Nov./Dec. 2007, doi: 10.1109/TIA.2007.908182.

[9] C. Meyer and R. W. De Doncker, "Design of a three-phase series resonant converter for offshore DC grids," in *Proc. IEEE Ind. Appl. Annu. Meeting*, 2007, pp. 216–223, doi: 10.1109/07IAS.2007.40.

[10] W. Chen, X. Wu, L. Yao, W. Jiang, and R. Hu, "A Step-up resonant converter for grid-connected renewable energy sources," *IEEE Trans. Power Electron.*, vol. 30, no. 6, pp. 3017–3029, Jun. 2015, doi: 10.1109/TPEL.2014.2336893.

[11] M. R. Islam, Y. Guo, J. Zhu, H. Lu, and J. X. Jin, "High-Frequency magnetic-link medium-voltage converter for superconducting generator-based high-power density wind generation systems," *IEEE Trans. Appl. Supercond.*, vol. 24, no. 5, Oct. 2014, Art. no. 5202605, doi: 10.1109/TASC.2014.2339137.

[12] M. R. Islam, M. A. Rahman, K. M. Muttaqi, and D. Sutanto, "A new magnetic-linked converter for grid integration of offshore wind turbines through MVDC transmission," *IEEE Trans. Appl. Supercond.*, vol. 29, no. 2, Mar. 2019, Art. no. 5400905, doi: 10.1109/TASC.2019.2895259.

[13] C. G. Dincan et al., "Design of a high-power resonant converter for DC wind turbines," *IEEE Trans. Power Electron.*, vol. 34, no. 7, pp. 6136–6154, Jul. 2019, doi: 10.1109/TPEL.2018.2876320.

[14] L. Shu et al., "A resonant ZVZCS DC–DC converter with two uneven transformers for an MVDC collection system of offshore wind farms," *IEEE Trans. Ind. Electron.*, vol. 64, no. 10, pp. 7886–7895, Oct. 2017, doi: 10.1109/TIE.2017.2694389.

[15] S. P. Engel, M. Stieneker, N. Soltau, S. Rabiee, H. Stagge, and R. W. De Doncker, "Comparison of the modular multilevel DC converter and the dual-active bridge converter for power conversion in HVDC and MVDC grids," *IEEE Trans. Power Electron.*, vol. 30, no. 1, pp. 124–137, Jan. 2015, doi: 10.1109/TPEL.2014.2310656.

[16] X. Xiang, X. Zhang, G. P. Chaffey, and T. C. Green, "An isolated resonant mode modular converter with flexible modulation and variety of configurations for MVDC application," *IEEE Trans. Power Del.*, vol. 33, no. 1, pp. 508–519, Feb. 2018, doi: 10.1109/TPWRD.2017.2735634.

[17] T.-F. Wu and Y.-K. Chen, "Modeling PWM DC/DC converters out of basic converter units," *IEEE Trans. Power Electron.*, vol. 13, no. 5, pp. 870–881, Sep. 1998, doi: 10.1109/63.712294.

[18] W. Long and S. Nilsson, "HVDC transmission: Yesterday and today," *IEEE Power Energy Mag.*, vol. 5, no. 2, pp. 22–31, Mar./Apr. 2007, doi: 10.1109/MPAE.2007.329175.

[19] M. A. Perez, S. Bernet, J. Rodriguez, S. Kouro, and R. Lizana, "Circuit topologies, modeling, control schemes, and applications of modular multilevel converters," *IEEE Trans. Power Electron.*, vol. 30, no. 1, pp. 4–17, Jan. 2015, doi: 10.1109/TPEL.2014.2310127.

[20] F. Z. Peng, "A generalized multilevel inverter topology with self voltage balancing," *IEEE Trans. Ind. Appl.*, vol. 37, no. 2, pp. 611–618, Mar./Apr. 2001, doi: 10.1109/28.913728.

[21] J.-S. Lai and F. Z. Peng, "Multilevel converters-a new breed of power converters," *IEEE Trans. Ind. Appl.*, vol. 32, no. 3, pp. 509–517, May/Jun. 1996, doi: 10.1109/28.502161.

[22] V. Yaramasu, B. Wu, P. C. Sen, S. Kouro, and M. Narimani, "High-power wind energy conversion systems: State-of-the-art and emerging technologies," *Proc. IEEE*, vol. 103, no. 5, pp. 740–788, May 2015, doi: 10.1109/JPROC.2014.2378692.

[23] A. Emadi, S. S. Williamson, and A. Khaligh, "Power electronics intensive solutions for advanced electric, hybrid electric, and fuel cell vehicular power systems," *IEEE Trans. Power Electron.*, vol. 21, no. 3, pp. 567–577, May 2006, doi: 10.1109/TPEL.2006.872378.

[24] Y. Chen, S. Zhao, Z. Li, X. Wei, and Y. Kang, "Modeling and control of the isolated DC–DC modular multilevel converter for electric ship medium voltage direct current power system," *IEEE J. Emerg. Sel. Top. Power Electron.*, vol. 5, no. 1, pp. 124–139, Mar. 2017, doi: 10.1109/JESTPE.2016.2615071.

[25] Landsman, "A unifying derivation of switching DC-DC converter topologies," in *Proc. IEEE Power Electron. Specialists Conf.*, 1979, pp. 239–243, doi: 10.1109/PESC.1979.7081032.

[26] B. Zhao, Q. Song, W. Liu, and Y. Sun, "Overview of dual-active-bridge isolated bidirectional DC–DC converter for high-frequency-link power-conversion system," *IEEE Trans. Power Electron.*, vol. 29, no. 8, pp. 4091–4106, Aug. 2014, doi: 10.1109/TPEL.2013.2289913.

[27] J. Everts, F. Krismer, J. Van den Keybus, J. Driesen, and J. W. Kolar, "Optimal ZVS modulation of single-phase single-stage bidirectional DAB AC–DC converters," *IEEE Trans. Power Electron.*, vol. 29, no. 8, pp. 3954–3970, Aug. 2014, doi: 10.1109/TPEL.2013.2292026.

[28] W. Chen, A. Huang, S. Lukic, J. Svensson, J. Li, and Z. Wang, "A comparison of medium voltage high power DC/DC converters with high step-up conversion ratio for offshore wind energy systems," in *Proc. IEEE Energy Convers. Congr. Expo.*, 2011, pp. 584–589, doi: 10.1109/ECCE.2011.6063822.

[29] F. Deng and Z. Chen, "Control of improved full-bridge three-level DC/DC converter for wind turbines in a DC grid," *IEEE Trans. Power Electron.*, vol. 28, no. 1, pp. 314–324, Jan. 2013, doi: 10.1109/TPEL.2012.2198835.

[30] R. Ayyanar, R. Giri, and N. Mohan, "Active input-voltage and load-current sharing in input-series and output-parallel connected modular DC-DC converters using dynamic input-voltage reference scheme," *IEEE Trans. Power Electron.*, vol. 19, no. 6, pp. 1462–1473, Nov. 2004, doi: 10.1109/TPEL.2004.836671.
[31] S. Kenzelmann, A. Rufer, D. Dujic, F. Canales, and Y. R. de Novaes, "Isolated DC/DC structure based on modular multilevel converter," *IEEE Trans. Power Electron.*, vol. 30, no. 1, pp. 89–98, Jan. 2015, doi: 10.1109/TPEL.2014.2305976.
[32] S. Kenzelmann, A. Rufer, D. Dujic, F. Canales, and Y. R. D. Novaes, "A versatile DC/DC converter based on modular multilevel converter for energy collection and distribution," in *Proc. IET Conf. Renewable Power Gener.*, 2011, pp. 1–6, doi: 10.1049/cp.2011.0126.
[33] S. Kenzelmann, "Modular dc/dc converter for dc distribution and collection networks," Ph.D. dissertation, Univ. Ecole Polytechnique Federale de, Lausanne, Switzerland, 2012.
[34] A. Bendre et al., "Design considerations for a soft-switched modular 2.4-MVA medium-voltage drive," *IEEE Trans. Ind. Appl.*, vol. 38, no. 5, pp. 1400–1411, Sep./Oct. 2002, doi: 10.1109/TIA.2002.802991.
[35] A. J. Watson et al., "A novel multilevel converter structure integrated into power systems and its performance evaluation," in *Proc. 13th Eur. Conf. Power Electron. Appl.*, Sep. 2009, pp. 1–10.
[36] H. Fan and H. Li, "High-Frequency transformer isolated bidirectional DC–DC converter modules with high efficiency over wide load range for 20 kVA solid-state transformer," *IEEE Trans. Power Electron.*, vol. 26, no. 12, pp. 3599–3608, Dec. 2011, doi: 10.1109/TPEL.2011.2160652.
[37] D. Montesinos-Miracle, M. Massot-Campos, J. Bergas-Jane, S. Galceran-Arellano, and A. Rufer, "Design and control of a modular multilevel DC/DC converter for regenerative applications," *IEEE Trans. Power Electron.*, vol. 28, no. 8, pp. 3970–3979, Aug. 2013, doi: 10.1109/TPEL.2012.2231702.
[38] G. J. Kish, M. Ranjram, and P. W. Lehn, "A modular multilevel DC/DC converter with fault blocking capability for HVDC interconnects," *IEEE Trans. Power Electron.*, vol. 30, no. 1, pp. 148–162, Jan. 2015, doi: 10.1109/TPEL.2013.2295967.
[39] R. W. A. A. De Doncker, D. M. Divan, and M. H. Kheraluwala, "A three-phase soft-switched high-power-density DC/DC converter for high-power applications," *IEEE Trans. Ind. Appl.*, vol. 27, no. 1, pp. 63–73, Jan./Feb. 1991, doi: 10.1109/28.67533.
[40] Z. Xing, X. Ruan, H. You, X. Yang, D. Yao, and C. Yuan, "Soft-Switching operation of isolated modular DC/DC converters for application in HVDC grids," *IEEE Trans. Power Electron.*, vol. 31, no. 4, pp. 2753–2766, Apr. 2016, doi: 10.1109/TPEL.2015.2448125.
[41] M. Abbasi and J. Lam, "A step-up transformerless, ZV–ZCS high-gain DC/DC converter with output voltage regulation using modular step-up resonant cells for DC grid in wind systems," *IEEE J. Emerg. Sel. Top. Power Electron.*, vol. 5, no. 3, pp. 1102–1121, Sep. 2017, doi: 10.1109/JESTPE.2017.2656919.
[42] V. Vorperian, "Quasi-square-wave converters: Topologies and analysis," *IEEE Trans. Power Electron.*, vol. 3, no. 2, pp. 183–191, Apr. 1988, doi: 10.1109/63.4348.
[43] A. Alfares, E. Afshari, M. Amirabadi, and B. Lehman, "A modular SCR-based DC-DC converter for medium-voltage direct-current (MVDC) grid applications," in *Proc. IEEE Energy Convers. Congr. Expo.*, 2017, pp. 5170–5177, doi: 10.1109/ECCE.2017.8096870.
[44] M. Khodabandeh, E. Afshari, and M. Amirabadi, "A family of Ćuk, zeta, and SEPIC based soft-switching DC–DC converters," *IEEE Trans. Power Electron.*, vol. 34, no. 10, pp. 9503–9519, Oct. 2019, doi: 10.1109/TPEL.2019.2891563.
[45] Z. Zhang, S. Tian, and K. D. T. Ngo, "Small-Signal equivalent circuit model of quasi-square-wave flyback converter," *IEEE Trans. Power Electron.*, vol. 32, no. 8, pp. 5885–5888, Aug. 2017, doi: 10.1109/TPEL.2017.2661320.
[46] X. Huang, F. C. Lee, Q. Li, and W. Du, "High-Frequency high-efficiency gan-Based interleaved CRM bidirectional buck/boost converter with inverse coupled inductor," *IEEE Trans. Power Electron.*, vol. 31, no. 6, pp. 4343–4352, Jun. 2016, doi: 10.1109/TPEL.2015.2476482.
[47] E. Afshari, M. Khodabandeh, and M. Amirabadi, "A single-stage capacitive AC-Link AC–AC power converter," *IEEE Trans. Power Electron.*, vol. 34, no. 3, pp. 2104–2118, Mar. 2019, doi: 10.1109/TPEL.2018.2841398.
[48] F. Krismer and J. W. Kolar, "Accurate power loss model derivation of a high-current dual active bridge converter for an automotive application," *IEEE Trans. Ind. Electron.*, vol. 57, no. 3, pp. 881–891, Mar. 2010, doi: 10.1109/TIE.2009.2025284.

ABDULGAFOR ALFARES (Member, IEEE) received the B.S. and M.S. degrees in electrical enginnering from Marquette University, Milwaukee, WI, USA, in 2011 and 2014 , respectively , and the Ph.D. degree in electrical engineering from Northeastern University, Boston , MA , USA, in 2020. Since May 2021, he joined the University of Hafr Albatin , Hafar Al-Batin, Saudi Arabia, as an Assistant Professor. His research interests include design, analysis, and control of power converters, renewable energy systems, and hybrid-electric aircraft propulsion. He is currently a Reviewer for the IEEE OPEN JOURNAL OF POWER ELECTRONICS.

BRAD LEHMAN (Senior Member, IEEE) is currently a Professor with the Department of Electrical and Computer Engineering, Northeastern University, Boston, MA, USA. He was a Hearin Hess Distinguished Assistant Professor with Mississippi State University, Starkville, MS, USA. Before becoming a Professor, he was the Head swimming and diving Coach with the Georgia Institute of Technology, Atlanta, GA, USA. He has been listed in the inaugural edition of the book The 300 Best Professors, (Princeton Review, 2012). His research interests include power electronics and controls, with applications to solar energy, LED lighting, battery energy management systems, and reliability. Dr. Lehman was the recipient of the 2015 IEEE (PELS) Power Electronics Society Modeling and Control Technical Achievement Award, the 2016 IEEE Standards Medallion, the 2018 IEEE Award for Achievement in Power Electronics Standards, and the 2019 IEEE PELS Harry A. Owen, Jr. Distinguished Service Award. He was an Editor-in-Chief of the IEEE TRANSACTIONS ON POWER ELECTRONICS, from 2013 to 2018, and currently is IEEE PELS VP for Products.

MAHSHID AMIRABADI (Senior Member, IEEE) received the B.S. degree in electrical engineering from Shahid Beheshti University, Tehran, Iran, in 2002, the M.S. degree in electrical engineering from the University of Tehran, Tehran, Iran, in 2006, and the Ph.D. degree in electrical engineering from Texas A&M University, College Station, TX, USA, in 2013. She joined the University of Illinois at Chicago, Chicago, IL, USA, in 2013 as an Assistant Professor. Since August 2015, she has been with Northeastern University, Boston, MA, USA, where she is currently an Associate Professor. Her main research interests and experience include universal power converters, renewable energy systems, variable speed drives, and wireless power transfer systems. Dr. Amirabadi was the recipient of the National Science Foundation CAREER Award in 2021. She is currently an Associate Editor for the IEEE TRANSACTIONS ON POWER ELECTRONICS.